Int. J. Heat Mass Transfer. Vol. 34, No. 3, pp. 625–632, 1991
Printed in Great Britain

0017–9310/91 $3.00 + 0.00

Transient behavior of an active thermal protection system

SHIGENAO MARUYAMA and TOSHIO AIHARA
Institute of Fluid Science, Tohoku University, Sendai 980, Japan

and

RAYMOND VISKANTA
School of Mechanical Engineering, Purdue University, West Lafayette, IN 47907, U.S.A.

(*Received* 12 *January* 1990)

Abstract—The transient behavior of an active thermal protection system consisting of a semi-infinite layer of a porous medium with gas injection is considered. During the early stages of heating, thermal penetration depth, surface temperature and surface heat flux do not depend on the gas injection velocity. As the heating time increases, the thermal penetration depth of the active thermal protection system reaches a constant value for each gas injection velocity, and the surface heat flux vanishes keeping the back face at a low temperature. However, the thermal penetration depth of conventional insulation without gas injection never reaches a constant value. Transient solid temperature distributions in the layer for two different surface boundary conditions are almost identical, except in the vicinity of the front surface.

1. INTRODUCTION

THERMAL protection and insulation are important for the cooling of rocket nozzles and re-entry vehicles, the protection of structures from high-intensity energy beams, and the design of furnaces for materials processing. A broad classification of the cooling techniques available was presented by Sutton *et al.* [1]. Among these techniques, porous media or fibrous media are the most commonly used types of insulation.

Matthews *et al.* [2] measured the transient insulation characteristics of porous media subjected to intense irradiation. At high temperature, the thermal conductance of the porous or fibrous media increases, because radiative heat transfer predominates over conduction. The insulation tiles of the space shuttle take advantage of the transient behavior of porous media, and a relatively thick insulation layer is required for protection during the long duration of re-entry.

Transpiration and mass transfer cooling is a well-known technique for protecting a structure from a high-temperature environment [3]. The technique was applied to protect a disaster prevention robot [4] by utilizing water injection through sintered metal fibers. The walls of the insulating system in a high-temperature environment are sometimes exposed to high-intensity irradiation, and the surface may be damaged because the vaporized liquid or coolant gas cannot protect the surface from the intense irradiation.

We consider a layer of semitransparent porous or fibrous material with a very fine structure, through which low-temperature gas is injected from a back face, as shown in Fig. 1. A large fraction of the incident radiation from the front face penetrates into the layer, and is scattered or absorbed by the porous medium. Since most of the incident radiation is not absorbed at the surface, the surface of the porous layer does not suffer directly from intense irradiation damage. The porous medium heated by the radiation which penetrates it is cooled efficiently by the injected gas.

The above-mentioned active thermal insulation system represents a problem of combined heat transfer of radiation, convection and conduction. A unique high-temperature heat transfer augmentation scheme utilizing porous media was proposed by Echigo [5], and Echigo *et al.* [6] studied lean combustion using the porous media. Aihara *et al.* [7] showed that high-efficiency solar gas heating can be attained by using compact fluidized bed solar receivers. An application of a packed bed for solar gas heating was studied by Flamant *et al.* [8].

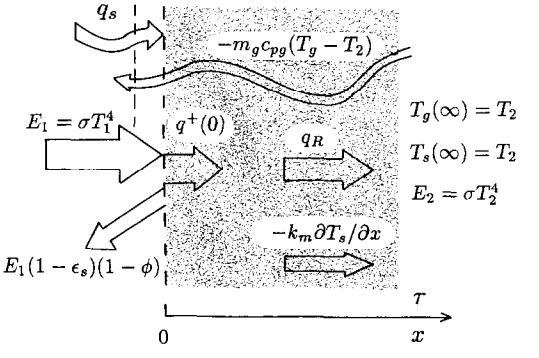

FIG. 1. Schematic of the physical model.

NOMENCLATURE

A_c, A_a, A_g conduction, heat advection, and convection parameter, equations (13)–(15), respectively
A_e surface area per unit volume, equation (4) [m^{-1}]
b, f backward and forward scattering fractions
c_{pg}, c_s specific heat of gas and porous material [J kg^{-1} K^{-1}]
d_p equivalent particle diameter of porous media [m]
E_b dimensionless black body emitted flux, equation (8)
E_1, E_2 radiation fluxes arriving at the front and back surface from the surroundings, σT_1^4, σT_2^4, Fig. 1 [W m^{-2}]
h_c effective heat transfer coefficient of porous medium [W m^{-2} K^{-1}]
k_m, k_g thermal conductivities of porous medium and gas, respectively [W m^{-1} K^{-1}]
m_g mass flux of injection gas [kg m^{-2} s^{-1}]
n_a apparent index of refraction of porous media
Nu_p Nusselt number based on particle diameter, $h_c d_p/k_g$
Pr Prandtl number of gas
Q dimensionless heat flux, $q/(E_1-E_2)$
q^+, q^- forward and backward radiation fluxes [W m^{-2}]
q_R radiation flux, $q^+ - q^-$, Fig. 1
q_s convective heat flux at front surface, Fig. 1 [W m^{-2}]
q_t total heat flux through porous media, equation (1), Fig. 1 [W m^{-2}]
Re_p particle Reynolds number, $m_g d_p/\eta$
T_1, T_2 radiation source temperature at the front surface and solid, and gas temperature at ∞, Fig. 1 [K]
T_g, T_s temperatures of gas and porous media [K]
t time [s]
t^* dimensionless time, equation (8)
x distance from front surface, Fig. 1
x_{p1}, x_{p2} thermal penetration depth, equation (20).

Greek symbols
ε_s surface emissivity of solid cross-section at front boundary, Fig. 1
η viscosity of gas [Pa s]
θ_s, θ_g dimensionless temperatures of porous medium and gas
ρ_s, ρ_g true density of porous material and density of gas [kg m^{-3}]
σ Stefan–Boltzmann constant [W m^{-2} K^{-4}]
σ_e extinction coefficient [m^{-1}]
τ optical depth, $\sigma_e x$
τ_{p1}, τ_{p2} dimensionless thermal penetration depth, equation (20)
ϕ porosity of porous media
ω_0 single scattering albedo of porous medium.

Other symbols
• time at which the value has reached 99% of the steady-state value
BC1, BC2 boundary conditions at the front surface, equation (17).

The authors have proposed a concept for an active thermal insulation system using a semitransparent porous medium [9]. For example, the heat flux through a 5-mm-thick layer, the front surface of which is subjected to an incident radiative flux of 1 MW m^{-2}, can be practically eliminated by keeping the back surface at room temperature. The authors [10] also demonstrated the effectiveness by utilizing a dissociating gas for the high-temperature active thermal insulation system. The present active thermal insulation system not only has remarkable steady-state characteristics but also transient ones. The active thermal insulation layer 10 mm thick reaches the steady state in a period 30 times shorter than in the case of a conventional porous layer without gas injection.

In this paper, the transient behavior of an active thermal insulation system consisting of a semi-infinite layer of porous medium is considered. Through numerical analysis, the transient behavior of the active thermal protection system, such as thermal penetration depth, local heat flux, and transient temperature distributions are investigated and compared with a conventional insulation system without gas injection. The effect of boundary conditions at the front surface on transient temperature distributions is also studied.

2. COMBINED HEAT TRANSFER MODEL AND NUMERICAL ANALYSIS

2.1. *Physical model and basic equations*

We consider a semi-infinite, one-dimensional layer of a semitransparent high porosity material as shown in Fig. 1. The front surface of the porous layer is exposed to a high intensity thermal radiation flux from time $t = 0$. A low-temperature gas of mass flux m_g is injected at the back face and flows towards the front surface. The radiation source in front of the surface

is characterized by the temperature T_1, and the temperature of the injected gas and the porous medium at $x = \infty$ is T_2 as shown in Fig. 1.

Under a very high-intensity irradiation, say, of 1–5 MW m^{-2}, the injected gas is subjected to a large temperature gradient as it passes through the porous medium. The temperature of the injected gas may increase by about 1000 K, and the thermophysical properties of the injected gas change substantially. The authors [10] showed that the effect of the thermophysical properties is rather small in the case of non-dissociating gas. Because the thickness of the porous layer is less than a few centimeters, the pressure drop across the layer is estimated to be a few hundred Pascal, and the pressure change in the porous layer is small enough compared with the static pressure (0.1 MPa). Considering the discussion above, the thermophysical properties of the gas are assumed to be independent of temperature and pressure change, and the values are estimated at T_2.

The total heat flux q_t through the porous layer is given by

$$q_t = -k_m \frac{\partial T_s}{\partial x} + q_R - m_g c_{pg}(T_g - T_2) \tag{1}$$

where the first and second term on the right-hand side of equation (1) represent conductive and radiative fluxes, respectively, and the heat fluxes are directed in the positive x-direction in Fig. 1. The third term, however, represents an advective transport, and the gas enthalpy flux is directed in the opposite direction. A large portion of the incident radiation flux penetrates into the porous layer as shown in Fig. 1, and is absorbed or scattered by the porous medium. The porous material heated by radiation and conduction is cooled efficiently by the injected gas.

Since the heat capacity of the gas per unit volume is of the order of 1/100 to 1/1000 of the porous medium, the transient term in the energy equation of the gas can justifiably be neglected. The gas is treated as radiatively nonparticipating, because the opacity of the gas in the layer is negligibly small compared to the porous medium, so the governing energy equation for the porous solid and the gas can be expressed as

$$(1-\phi)\rho_s c_s \frac{\partial T_s}{\partial t} = \frac{\partial}{\partial x}(-q_t) = k_m \frac{\partial^2 T_s}{\partial x^2} - \frac{\partial q_R}{\partial x} + m_g c_{pg} \frac{\partial T_g}{\partial x} \tag{2}$$

$$-m_g c_{pg} \frac{\partial T_g}{\partial x} = A_e h_e (T_s - T_g) \tag{3}$$

where A_e and h_e are the effective surface area per unit volume and the heat transfer coefficient of the gas and the solid, respectively. We assume that the solid matrix can be represented by a packed bed of spherical monodisperse particles of diameter d_p. Thus

$$A_e = 6(1-\phi)/d_p. \tag{4}$$

The empirical correlation proposed by Huber and Jones [11] is adopted for estimating the heat transfer coefficient of the porous medium

$$Nu_p = 0.054 Re_p^{1.48}, \quad 0.7 < Re_p < 16. \tag{5}$$

As far as the radiative transfer is concerned, there have been many approximate methods [12] proposed for predicting the radiant heat flux q_R. The two-flux approximation is adopted in the analysis of the radiative transfer

$$\left.\begin{aligned} \frac{1}{2}\frac{dq^+}{d\tau} &= -1(-f\omega_0)q^+ + \omega_0 b q^- + n_a^2(1-\omega_0)\sigma T_s^4 \\ -\frac{1}{2}\frac{dq^-}{d\tau} &= -1(-f\omega_0)q^- + \omega_0 b q^+ + n_a^2(1-\omega_0)\sigma T_s^4 \end{aligned}\right\} \tag{6}$$

where n_a is the effective refractive index of the porous material, originally derived by Maxwell–Garnett [13]. In general, the radiative properties are dependent on the wavelength of the radiation; however, for simplicity the porous material is assumed to be gray. Equations (2) and (6) are related by the following equation:

$$\frac{\partial q_R}{\partial \tau} = 2(1-\omega_0)(-q^+ - q^- + 2n_a^2 \sigma T_s^4). \tag{7}$$

2.2. *Dimensionless expression and boundary conditions*

The present model considers the situation when there is a very large temperature difference across the medium, and the front surface is subjected to very intense irradiation. Since the present model considers the semi-infinite layer of a porous medium, we cannot use the thickness of the layer as the reference length as has been done in previous papers [9, 10]. Considering the above discussion, the following dimensionless values are introduced using T_1, T_2, E_1, E_2, and the inverse of the extinction coefficient $1/\sigma_e$ as a reference length

$$\left.\begin{aligned} \theta_s = (T_s - T_2)/(T_1 - T_2), \quad \theta_g = (T_g - T_2)/(T_1 - T_2) \\ Q_R = q_R/(E_1 - E_2), \quad Q^+ = q^+/(E_1 - E_2) \\ Q^- = q^-/(E_1 - E_2), \quad t^* = \frac{t(E_1 - E_2)\sigma_e}{(1-\phi)\rho_s c_s} \\ E_b = \frac{\sigma T_s^4}{E_1 - E_2}. \end{aligned}\right\} \tag{8}$$

Thus, basic equations (2), (3), (6), and (7) can be rewritten as follows:

$$\frac{\partial \theta_s}{\partial t^*} = A_c \frac{\partial^2 \theta_s}{\partial \tau^2} - \frac{\partial Q_R}{\partial \tau} + A_a \frac{\partial \theta_g}{\partial \tau} \tag{9}$$

$$\frac{\partial \theta_g}{\partial \tau} = -A_g(\theta_s - \theta_g) \tag{10}$$

$$\left.\begin{aligned}\frac{1}{2}\frac{\mathrm{d}Q^+}{\mathrm{d}\tau} &= -(1-f\omega_0)Q^+ + \omega_0 b Q^- + (1-\omega_0)E_b \\ -\frac{1}{2}\frac{\mathrm{d}Q^-}{\mathrm{d}\tau} &= -(1-f\omega_0)Q^- + \omega_0 b Q^+ + (1-\omega_0)E_b\end{aligned}\right\} \quad (11)$$

$$\frac{\partial Q_R}{\partial \tau} = 2(1-\omega_0)(-Q^+ - Q^- + 2E_b) \quad (12)$$

where A_c, A_a, and A_g in equations (9) and (10) are conduction, advection, and convection parameters, respectively, and are expressed as

$$A_c = \frac{k_m \sigma_e (T_1 - T_2)}{E_1 - E_2} \quad (13)$$

$$A_a = \frac{m_g c_{pg}(T_1 - T_2)}{E_1 - E_2} \quad (14)$$

$$A_g = \frac{6(1-\phi)Nu_p}{\sigma_e d_p Pr\, Re_p}. \quad (15)$$

The dimensionless parameters are based on radiant heat flux which is a dominant flux of the present thermal protection system.

The irradiation at the front surface at a time $t > 0$ is $E_1 = \sigma T_1^4$, and a fraction of the flux is reflected, while the remaining part of the flux penetrates into the porous layer. Thus, the radiative boundary condition at the surface ($\tau = 0$) is expressed in the same manner as in the previous report [9]

$$Q^+ = \frac{\{\phi + \varepsilon_s(1-\phi)\}E_1}{E_1 - E_2} \quad \text{at} \quad \tau = 0. \quad (16)$$

In general, the front surface exposed to a high-temperature environment is also subjected to the convective heat flux q_s. The convective flux represents a rather large fraction of the surface heat flux, especially for a rocket nozzle and the space shuttle [14]. On the other hand, the transpired gas reduces the convective heat flux at the front surface. It is difficult to estimate the convective heat flux when the transpired gas is not in thermal equilibrium with the porous solid [9]. Hence, the following two extreme boundary conditions are considered for the present model.

(1) Boundary condition 1 (BC1): only the radiative heat flux is considered and the convective heat flux q_s at the front surface is neglected.

(2) Boundary condition 2 (BC2): the convective heat transfer coefficient at the front surface is very large and the surface temperature is in thermal equilibrium with the outer boundary.

These boundary conditions are expressed in a dimensionless form as follows:

$$\left.\begin{aligned}-\frac{\partial \theta_s}{\partial \tau} &= \frac{(1-\phi)\varepsilon_s \sigma [T_1^4 - T_s^4(0)]}{k_m (T_1 - T_2)\sigma_e} &&: \text{BC1} \\ \theta_s &= 1 &&: \text{BC2}\end{aligned}\right\} \quad \text{at} \quad \tau = 0. \quad (17)$$

The gas and solid temperatures and radiation flux are in thermal equilibrium at $\tau = \infty$, so, the boundary conditions are

$$\theta_s = \theta_g = Q_R = 0 \quad \text{for} \quad \tau = \infty. \quad (18)$$

The initial temperatures of the porous medium and the gas are both assumed to be T_2. Then, the initial conditions are

$$\theta_s = \theta_g = Q_R = 0 \quad \text{at} \quad \tau^* = 0. \quad (19)$$

The solutions of equations (9)–(11) are obtained numerically using a finite-difference scheme with an iterative procedure and unequal grid sizes, which is a similar procedure to the previous numerical analysis [9]. In the present analysis, the calculation regime is extended with increasing time in order that the condition at $\tau = \infty$ be satisfied. Namely, the calculation regime is taken more than twice the thermal penetration depth τ_{p2} defined in the following section.

3. RESULTS AND DISCUSSION

There are numerous publications in the literature concerned with the radiative properties of porous or fibrous material (for example, Kurosaki *et al.* [15]), but only a few publications report both the thermal and radiative properties of high-temperature porous materials. In the present numerical analysis, a porous zirconia, the thermal and radiative properties of which were measured by Matthews *et al.* [2], is chosen as an example [9]. The thermophysical and radiative properties of the porous medium are listed in Table 1. The radiation source temperature T_1 is set at 3000 K, which corresponds to an incident radiation flux of $E_1 = 4.6$ MW m^{-2}. The temperature at $\tau = \infty$ is set at 300 K. According to the authors' previous work [10], hydrogen is used as the transpired gas of the present numerical example. The mass flux is chosen in order that the advection parameter be $A_a = 2.0$–0.2, because the active thermal protection system is most effective [10] when $A_a > 1.0$. The dimensionless parameters used in the present numerical analysis and corresponding dimensional values are listed in Table 2.

Table 1. Thermophysical and radiation properties of porous zirconia

Thermophysical properties	
$c_s = 1.75 \times 10^3$ J kg^{-1} K^{-1}	$\rho_s = 5.6 \times 10^3$ kg m^{-3}
$k_m = 7.0 \times 10^{-2}$ W m^{-1} K^{-1}	$d_p = 10^{-4}$ m
$\phi = 0.9$	
Radiation properties	
$\sigma_e = 8.969 \times 10^3$ m^{-1}	$b = 0.2506$
$n_s = 1.6$	$n_g = 1.0$
$\omega_0 = 0.99$	$\varepsilon_s = 0.35$

Table 2. Dimensionless and dimensional parameters of calculation conditions

A_c =	0.369			
A_a = 2.0	1.0	0.5	0.2	
A_g = 0.085	0.061	0.044	0.028	
m_g = 0.238	0.119	0.059	0.024	kg m^{-2} s^{-1}
t^* = 1		τ = 1		
t = 6.4×10^{-2} s		x = 0.11 mm		
T_1 = 3000 K		T_2 = 300 K		
E_1 = 4.6 MW m^{-2}		E_2 = 460 W m^{-2}		

3.1. *Transient characteristics of thermal penetration depth*

The thermal penetration depth is an important parameter for determining the thickness of the insulation layer. In the present analysis, the thermal penetration depth is defined as the point where the solid temperature is reduced to the value $\theta_s = 0.1$ or 0.01 as is expressed by the following equations:

$$\left.\begin{aligned} \theta_s = 0.1 \quad &\text{at} \quad x = x_{p1}, \quad \tau = \tau_{p1} \\ \theta_s = 0.01 \quad &\text{at} \quad x = x_{p2}, \quad \tau = \tau_{p2}. \end{aligned}\right\} \tag{20}$$

The transient behavior of the thermal penetration depth for various advection parameters A_a is shown in Figs. 2(a) and (b). The penetration depths without gas injection ($A_a = 0$) and for pure conduction (for BC2) are also plotted in these figures for comparison.

The thermal penetration depth for case BC2 in the very early stages is identical with that of pure conduction. The boundary conditions at the front surface affect the thermal penetration depth during these stages. Subsequently, the depth for the radiation and conduction model increases rapidly compared with that for pure conduction. This trend is remarkable for τ_{p2}. During the early stages of heating, the effect of gas injection is very small, and the penetration depths τ_{p1} and τ_{p2} for $A_a \neq 0$ are identical to those for $A_a = 0$.

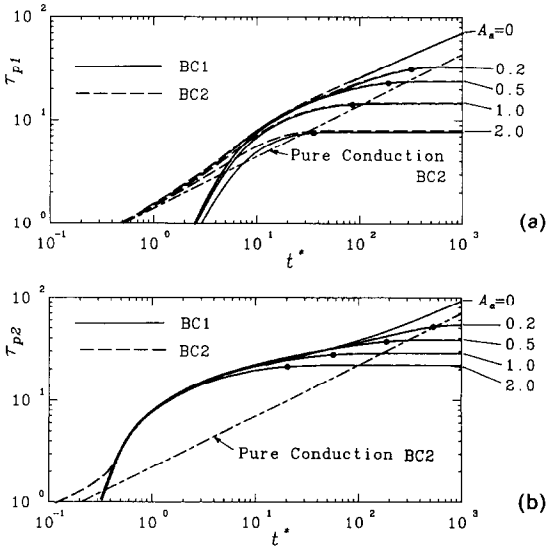

FIG. 2. Transient variation of thermal penetration depths τ_{p1} and τ_{p2}.

As the heating time increases, the penetration depth with gas injection reaches a steady state, whereas the depth for the pure conduction and radiation conduction models never reaches a steady-state condition. One of the main features of the active thermal protection system is its steady-state thermal penetration depth. The difference in the boundary conditions at the front surface is negligibly small, except in the early stage of heating. This is mainly due to the large extinction coefficient of the porous layer.

The symbol • in Fig. 2 represents the time when the value has reached 99% of the steady-state value. The larger the advection parameter A_a, the sooner the penetration depth reaches steady state. Comparison between Figs. 2(a) and (b) shows that the time when τ_p becomes independent of time is strongly affected by the advection parameter particularly for τ_{p2}.

3.2. *Transient heat flux and solid and gas temperature at the front surface*

Transient solid temperatures at the front surface for case BC1 are plotted in Fig. 3. In the early stages of heating, the surface temperature is independent of the advection parameter A_a. After the surface temperature reaches the steady-state condition, the steady-state value decreases with increasing A_a. It is noted that steady-state temperature is reached even for the case without gas injection ($A_a = 0$).

Heat advection by gas injection plays an important role in the active thermal protection system by reducing the surface temperature and thermal penetration depth. The dimensionless gas temperatures at the

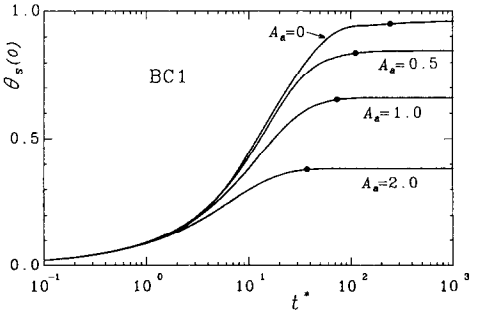

FIG. 3. Transient variation of dimensionless solid temperature at the front surface (boundary condition 1).

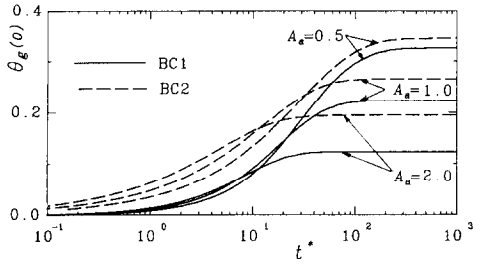

FIG. 4. Transient dimensionless gas temperature at the front surface.

front surface are plotted in Fig. 4 for various advection parameters and boundary conditions. The exit gas temperature is affected by the solid temperature in the vicinity of the front surface, and the solid temperature in that region is strongly influenced by the boundary conditions. Consequently, the gas temperature is strongly affected by the boundary condition. The trend is especially remarkable for a large advection parameter A_a.

Comparison of Figs. 3 and 4 shows that there is a large difference between solid and gas temperatures at the front surface. This fact suggests that an assumption of thermal equilibrium between the gas and porous solid, which is adopted in some papers on heat transfer in porous media, is inappropriate for the present active thermal protection.

The dimensionless total heat flux at the front surface is defined as follows:

$$Q_t(0) = -A_c \frac{\partial \theta_s}{\partial \tau} + Q_R - A_a \theta_g \quad \text{at} \quad \tau = 0. \quad (21)$$

In Fig. 5, the transient dimensionless heat fluxes with various advection parameters are plotted for case BC1. The transient total heat flux in the porous layer is a function of time and location, and approaches zero as $\tau \to \infty$. The surface heat flux $Q_t(0)$ is a maximum as $t^* \to 0$. When t^* is small, the radiant heat flux predominates over conduction and advection heat fluxes, because the solid temperature is small. Hence, the heat flux is constant, and is independent of the advection parameter. The heat flux decreases with increasing heating time, and finally becomes zero throughout the layer. This reduction in the total heat flux is faster for large A_a.

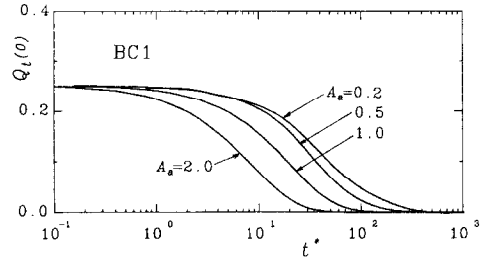

FIG. 5. Dimensionless total heat flux at the front surface for boundary condition 1.

In conventional insulation systems, there is heat transfer across the system when there is a temperature difference in the insulation across the layer. Comparison of Figs. 2(b) and 5 shows that the present active thermal protection system can reduce the heat flux through the layer to zero, maintaining a temperature difference of 2700 K within the layer of $\tau = 21$ (2.4 mm) for $A_a = 2.0$.

3.3. *Transient temperature distribution in the porous layer*

Variations of transient temperature distributions in the porous solid T_s (K) are expressed by three-dimensional plots of distance from the front surface (mm) and heating time (s) in Fig. 6. Figures 6(a) and (b) represent the case of the advection parameter $A_a = 1.0$ ($m_g = 0.12$ kg m^{-2} s^{-1}) with boundary conditions BC2 and BC1, respectively. The transient temperature distributions of the conventional porous layer with gas injection are plotted in Fig. 6(c) for comparison. The variation in the thermal penetration depths x_{p1} and x_{p2} (mm) are plotted in Figs. 6(a)–(c). The symbol • denotes the time when the thermal penetration depth has reached 99% of the steady-state value.

A comparison of Figs. 6(a) and (b) reveals that the temperature distributions for the different boundary conditions are almost identical, except in the vicinity of the front surface, although these two boundary conditions are completely different. The thermal penetration depths x_{p1} and x_{p2} reach steady-state values of 1.6 and 3.2 mm, respectively, and the values are identical for the two boundary conditions (Figs. 6(a) and (b)). Also, it should be noted that the temperature distribution reaches the steady state within 5 s.

The conventional insulation without gas injection, as shown in Fig. 6(c), on the other hand, has a completely different transient temperature distribution. Heat penetrates into the layer with time, and the temperature distribution never reaches steady state. The penetration depths x_{p1} and x_{p2} at $t = 100$ s are 9.3 and 12.5 mm, respectively, and the values are very large compared with those of the present active thermal protection system.

4. CONCLUSIONS

The transient behavior of an active thermal protection system consisting of a semi-infinite layer of a porous medium with gas injection was considered. Numerical analyses were carried out for transient heat transfer by combined conduction, convection and radiation for the case of a zirconia porous material and hydrogen injected at the back face. The characteristic radiation source temperature at the front surface is 3000 K or an irradiation of 4.6 MW m^{-2}.

In the early stages of heating, the thermal penetration depth is affected by the boundary conditions at the front surface, but are independent of the mass flux of the injected gas. As the heating time increases,

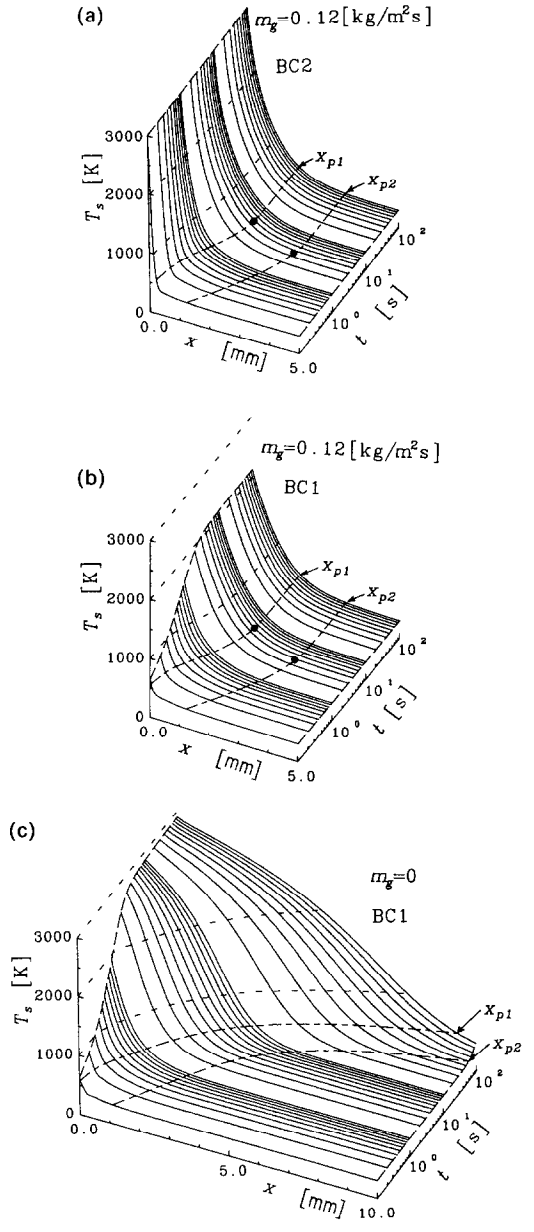

FIG. 6. (a) Transient temperature distributions of porous solid with gas injection (boundary condition 2). (b) Transient temperature distributions of porous solid with gas injection (boundary condition 1). (c) Transient temperature distributions in conventional porous insulation layer without gas injection.

the thermal penetration depth of the active thermal protection system reaches the steady state, and the value is independent of boundary conditions, whereas the thermal penetration depth of the conventional insulation never reaches steady state.

Solid temperature and total heat flux at the front surface are independent of the gas injection velocity during the initial stages of heating; subsequently, the former reaches a steady-state value, and the latter decays to zero with increasing heating time. The proposed active thermal protection system can maintain a temperature difference of 2700 K within a layer 2.4 mm thick (mass flux = 0.24 kg m^{-2} s^{-1}) without transfer of heat across the layer.

The transient temperature distributions for different boundary conditions at the front surface are almost identical except in the vicinity of the front surface. The thermal penetration is confined to a very small layer thickness (3.2 mm for mass flux = 0.12 kg m^{-2} s^{-1}), and this condition is attained within 5 s. However, the heat penetrates into the layer with increased heating time in the case of conventional insulation without gas injection.

REFERENCES

1. G. P. Sutton, W. R. Wagner and J. D. Seader, Advanced cooling of rocket engines, *Aeronaut. Astronaut.* **4,** 60–71 (1966).
2. L. K. Matthews, R. Viskanta and F. P. Incropera, Combined conduction and radiation heat transfer in porous materials heated by intense solar radiation, *ASME J. Solar Energy Engng* **107,** 29–34 (1985).
3. J. P. Hartnett, Mass transfer cooling. In *Handbook of Heat Transfer Applications* (Edited by W. M. Rohsenow, J. P. Hartnett and E. N. Ganic), 2nd Edn, pp. 1-1–1-109. McGraw-Hill, New York (1985).
4. T. Yano, E. Matsushima and S. Fuchigami, Thermal protection for disaster prevention robot by transpiration cooling, *Proc. 25th Natn. Heat Transfer Symp.*, Japan, Vol. 2, pp. 187–189 (1989).
5. R. Echigo, Effective conversion method between gas enthalpy and thermal radiation and its application to industrial furnaces, *Trans. JSME* Ser. B **48,** 2315–2323 (1982).
6. R. Echigo, M. Kurusu, K. Ichimiya and Y. Yoshizawa, Combustion augmentation of extremely low calorific gases (application of the effective energy conversion method from gas enthalpy to thermal radiation), *Trans. JSME* Ser. B **51,** 1136–1143 (1985).
7. T. Aihara, S. Maruyama and J. S. Choi, High temperature solar gas heating by compact fluidized-bed receivers, Mem. Inst. High Speed Mech., Tohoku University, Vol. 61, pp. 29–46 (1989).
8. G. Flamant, T. Menigault and D. Shwander, Combined heat transfer in a semitransparent multilayer packed bed, *ASME J. Heat Transfer* **110,** 463–467 (1988).
9. S. Maruyama, R. Viskanta and T. Aihara, Active thermal protection system against intense irradiation, *AIAA J. Thermophys. Heat Transfer* **3,** 389–394 (1989).
10. S. Maruyama, R. Viskanta and T. Aihara, Analysis of an active high temperature thermal insulation system, *Int. J. Heat Fluid Flow* (in press).
11. M. L. Huber and M. C. Jones, A frequency response study of packed bed heat transfer at elevated temperatures, *Int. J. Heat Mass Transfer* **31,** 843–853 (1988).
12. M. P. Menguc and R. Viskanta, Comparison of radiative transfer approximations for a highly forward scattering planar medium, *J. Quant. Spectrosc. Radiat. Transfer* **29,** 381–394 (1983).
13. H. Reiss, *Radiative Transfer in Nontransparent, Dispersed Media*, pp. 136–138. Springer, Berlin (1988).
14. J. N. Moss, G. A. Bird and V. K. Dogra, Nonequilibrium thermal radiation for an aeroassist flight experiment vehicle, AIAA Paper No. 88-0081 (1988).
15. Y. Kurosaki, M. Takeuchi, T. Kashiwagi and J. Yamada, Development of measuring method for radiative properties of fibrous porous media, *Proc. ASME/JSME Thermal Engng Joint Conf.* (Edited by P. J. Marto and I. Tanasawa), Vol. 4, pp. 319–325. ASME/JSME, New York/Tokyo (1987).

COMPORTEMENT TRANSITOIRE D'UN SYSTEME DE PROTECTION THERMIQUE ACTIF

Résumé—On considère le comportement transitoire d'un système de protection thermique actif qui consiste en une couche semi-infinie poreuse avec injection de gaz. Pendant les premiers temps de chauffage, la profondeur de pénétration thermique, la température de la surface et le flux thermique surfacique ne dépendent pas de la vitesse d'injection du gaz. Quand le temps de chauffage augmente, la profondeur de pénétration thermique atteint une valeur constante qui dépend de la vitesse d'injection du gaz et le flux de chaleur à la surface diminue pour atteindre la face arrière à faible température. La longueur de pénétration thermique d'une isolation conventionnelle sans injection de gaz n'atteint jamais une valeur constante. Les distributions variables de température dans la couche pour deux conditions différentes sur la surface sont pratiquement identiques, excepté au voisinage de la surface amont.

DAS INSTATIONÄRE VERHALTEN EINES AKTIVEN SYSTEMS ZUM THERMISCHEN SCHUTZ

Zusammenfassung—Das instationäre Verhalten eines aktiven Systems zum thermischen Schutz wird untersucht. Es besteht aus einer halbunendlichen porösen Schicht mit Gasinjektion. Zu Beginn der Beheizung hängen die thermische Eindringtiefe, die Oberflächentemperatur und die Wärmestromdichte an der Oberfläche nicht von der Gasinjektionsgeschwindigkeit ab. Für längere Beheizungszeiten erreicht die thermische Eindringtiefe für eine bestimmte Gasinjektionsgeschwindigkeit einen konstanten Wert, die Wärmestromdichte an der Oberfläche verschwindet. Im Gegensatz dazu erreicht die thermische Eindringtiefe bei herkömmlichen Wärmedämmungen ohne Gasinjektion niemals einen konstanten Wert. Die instationären Temperaturverteilungen im Feststoff der porösen Schicht sind für zwei unterschiedliche Randbedingungen an der Oberfläche nahezu identisch—außer in unmittelbarer Nähe der vorderen Oberfläche.

ПЕРЕХОДНЫЕ ХАРАКТЕРИСТИКИ АКТИВНЫХ ТЕПЛОЗАЩИТНЫХ СИСТЕМ

Аннотация—Исследуются переходные характеристики активных теплозащитных систем, состоящих из полуограниченного слоя пористой среды с вдувом газа. На ранних стадиях нагрева глубина теплового проникновения, температура поверхности и тепловой поток на ней не зависят от скорости вдува газа. С ростом времени нагрева глубина теплового проникновения активных систем теплозащиты достигает постоянного значения при любой скорости вдува газа и тепловой поток на поверхности исчезает, в результате чего на задней стенке сохраняется низкая температура. В случае же обыкновенной изоляции при отсутствии вдува газа глубина теплового проникновения не достигает постоянной величины. Нестационарные распределения температур твердого тела в слое при двух различных граничных условиях на поверхности являются почти одинаковыми, за исключением окрестности передней поверхности.